Volume 3
Number 11
November 2024
Pages 1467–1644

Environmental Science Advances

rsc.li/esadvances

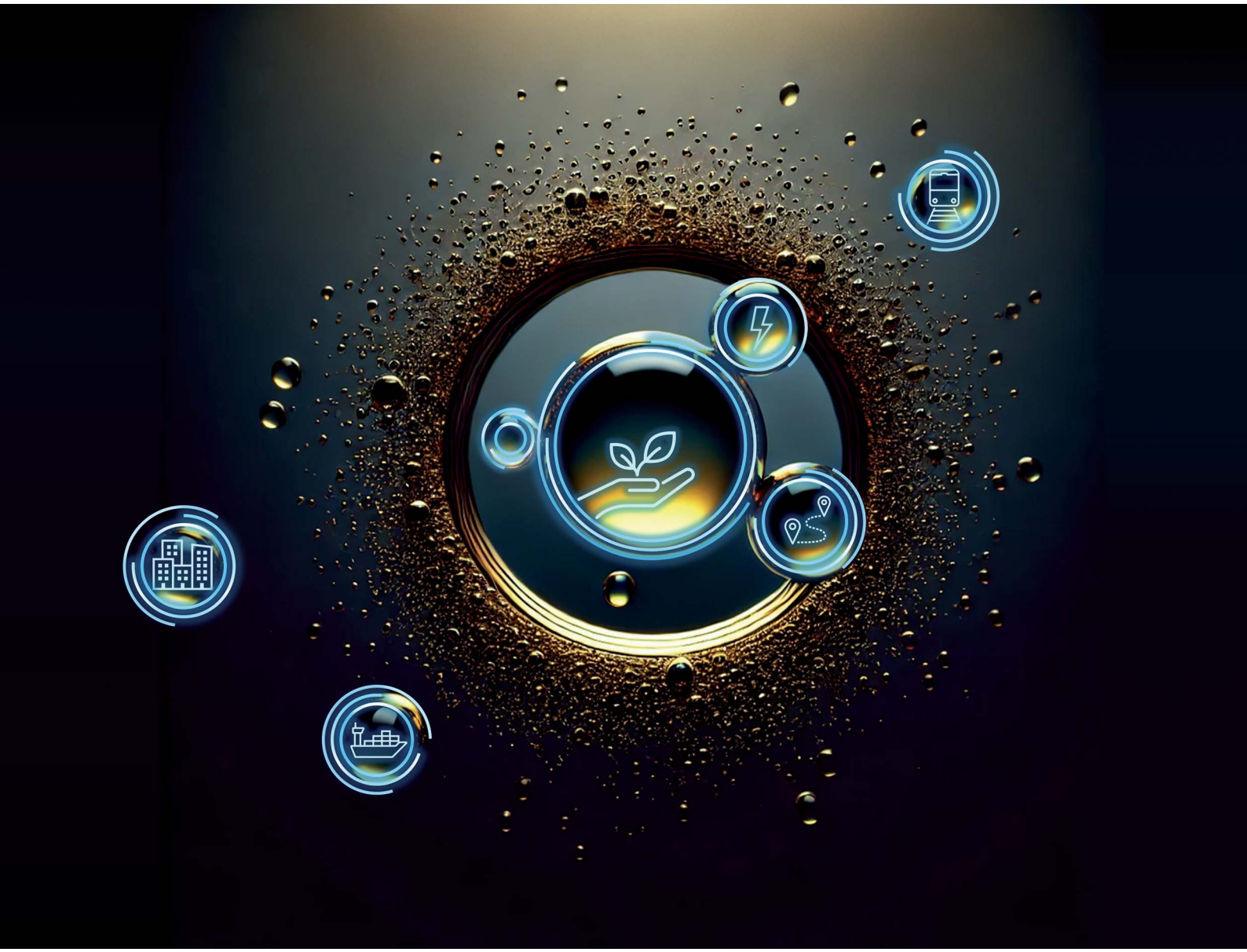

ISSN 2754-7000

ROYAL SOCIETY OF CHEMISTRY

PAPER
Felina Armbruster *et al.*
Investigations on particle emissions of large-bore engines powered by natural gas and hydrogen

Environmental Science Advances

ROYAL SOCIETY OF CHEMISTRY

PAPER

View Article Online
View Journal | View Issue

Cite this: *Environ. Sci.: Adv.*, 2024, **3**, 1524

Investigations on particle emissions of large-bore engines powered by natural gas and hydrogen†

Felina Armbruster, *[a] Alexander Gelner, [b] Andreas Zepf,[a] Maximilian Prager,[a] Martin Härtl [a] and Malte Jaensch[a]

In an effort to mitigate the impact of climate change, *e.g.*, by reducing the emission of greenhouse gases, hydrogen is becoming an increasingly attractive alternative energy source, replacing conventional long-chain hydrocarbon fuels in the energy and transport sector. While there is a shift in individual transport towards battery-electric applications, the maritime and energy production sectors rely on a high energy density and time- and location-independent availability of the energy carrier. Therefore, large-bore engines powered by renewable fuels have the potential to shift the industry towards a climate-neutral operation. Besides the emission of greenhouse gases, internal combustion engines are known for emitting pollutant emissions, harming human health and the environment. Research on particle emissions of natural gas and hydrogen engines has mainly focused on automotive and heavy-duty applications. Hence, this study investigates particle emissions of a large-bore single-cylinder research engine powered by hydrogen, compared to natural gas, for the first time. Investigations on particles with a diameter as low as 10 nm showed particle numbers of 10^4 to 10^5 # cm^{-3}, unexpectedly achieving slightly higher particle numbers in hydrogen than in natural gas operations. This is due to particles from lubricant oil and a stronger fuel interaction with the liner oil film in hydrogen operation, demonstrated within a 3D-CFD simulation. The concentrations are still lower by several orders of magnitude than in long-chain hydrocarbon fuel operations of identical engines. An extended emissions analysis based on the gaseous components THC, CO, and CO_2 shows the negligible carbonaceous emissions induced by these oil-based particles.

Received 13th June 2024
Accepted 9th August 2024

DOI: 10.1039/d4va00200h

rsc.li/esadvances

Environmental significance

The urgent need to minimize global CO_2 emissions has led to the exploration of alternative fuels such as hydrogen and natural gas. These fuels are being considered for large engine applications in ships, railways, and the energy production sector. They promise minimal to zero CO_2 emissions, offering a viable path toward decarbonization. However, besides focusing on greenhouse gas reductions, it is crucial to address pollutant emissions, which pose significant risks to human health and the environment. This study provides insights into pollutant emissions from a large bore engine powered by natural gas and hydrogen. By examining these emissions, this research highlights the environmental impact of such engines and ensures a holistic advancement towards sustainable and cleaner engine technologies.

Motivation

Today's interdisciplinary landscape is evermore shaped by a heightened environmental consciousness and a global push for sustainable practices.[1] To forward global decarbonization, developments are undertaken in all sectors of everyday life.[1] Besides climate change, governments also aim for air pollution control – especially in urban areas.[2] The transport sector, *e.g.*, road traffic, has recently been at the forefront of discussion, emitting both CO_2 and pollutants *via* the combustion of fossil fuels in internal combustion engines (ICEs).[3–5] Fig. 1 underlines this statement by showing the sector distribution of CO_2 and several pollutant emissions.[6–8] While CO_2 is a greenhouse gas, particle emissions contribute to air pollution, harming the human body and the environment.[9–13] Therefore, different regulations limit particle emissions caused by road traffic.[14] Although these regulations reflect regional priorities, they underscore a shared commitment to curb pollutant emissions.[14] Triggered by these regulations, many investigations were conducted covering automotive and heavy-duty diesel engine particle emissions regarding total particulate mass (PM), particle number (PN), particle size distribution, carbon mass, surface and effective density, morphology, and structure.[15–22] First, it is possible to develop strategies that can directly

[a]*Technical University of Munich, Institute of Sustainable Mobile Powertrains, Schragenhofstraße 31, 80992, Germany. E-mail: felina.armbruster@tum.de*

[b]*Technische Hochschule Ingolstadt, Esplanade 10, 85049 Ingolstadt, Germany*

† Electronic supplementary information (ESI) available. See DOI: https://doi.org/10.1039/d4va00200h

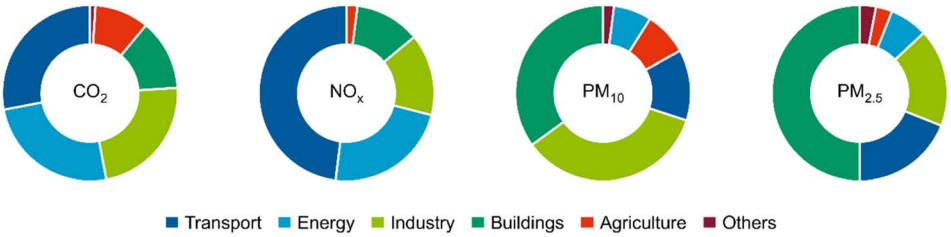

Fig. 1 Share on global CO_2, NO_x, PM_{10}, and $PM_{2.5}$ emission of different sectors. Data taken from ref. 5–7.

improve the combustion reaction and the after-treatment of exhaust gases. Additionally, alternative fuels such as biodiesel can replace fossil diesel and gasoline since, due to their molecular composition and different physical properties, they lead to a reduction in the size of emitted particles.[23–25] The combustion of biodiesel leads to decreased particulate matter, shifting the size distribution to smaller particles.[23–25] Investigations on the synthetic diesel substitute fuel oxymethylene ether (OME) show a solution to the NO_x-PN tradeoff as the lack of intramolecular C–C bonds inhibits the agglomeration of soot precursors.[15,18,19] The current shift towards battery-electric vehicles in the car segment, and occasionally also for heavy-duty applications, shows a comprehensive reduction in propulsion-driven particle emission. In the car segment, particle emissions induced by brake and tire wear are planned to be considered with the upcoming Euro 7 legislation.[26] Consequently, battery electric vehicles will also be subject to particulate emission assessments under this new definition.[26] However, the electrification of applications in the maritime and power sectors is currently not feasible, considering the energy density of state-of-the-art batteries. The temporal and local fluctuation of renewable sources, *e.g.*, solar and wind power, add to availability uncertainties, which are crucial in these sectors. Addressing availability uncertainties from renewable energy sources, Power-to-Gas (PtG) concepts propose intermediate storage of produced energy in gases, *e.g.*, hydrogen, and need-based utilization or reconversion to electricity.[27,28]

Furthermore, there are distinct demands for heavy-duty applications, such as extended service life, high full-load capabilities, and selective efficiency optimization while necessitating a simple fuel storage infrastructure.[29,30] This leads to large-bore engines still mainly being considered in ships, rail transportation, and heat and power plants in the future – their use comprehensively impacts the environment and climate.[31] Nowadays, these engines are operated mainly on heavy fuel oil distillates or diesel.[27,31] Aiming for sustainable heat, electricity, and transport powered by clean energy,[1,2] these conventional fuels are increasingly criticized for their exhaust gas emissions.[31] This discussion propels the research on alternative fuels like natural gas and hydrogen into the forefront of energy carriers, as they enable reduced to zero CO_2 emissions.[28,32–34] However, natural gas engines can also emit high levels of methane due to fuel slip, which contributes to the greenhouse gas effect.[28,34] In addition to the harmful effect of CO_2 and CH_4 on the climate, the impact of exhaust pollutants on human health must also be considered for these fuels.[35] As both natural gas and hydrogen share the lack of C–C-bonds with OME, the particle emissions are assumed to remain at a significantly lower level than for (bio-) diesel fuel. In this order of magnitude, the influence of lubricating oil on particulate emissions gains importance.[36] Despite the publication of Ristovski *et al.*[37] on a natural gas large-bore engine, research focuses on automotive or heavy-duty applications. Therefore, this study covers the particle emission of a large-bore engine operated on natural gas and hydrogen. One of the aims of this paper is to fill the literature gap related to the particulate emissions of large-bore engines, by providing researchers with solid emission data that can support decision-makers. Moreso, the necessity to adapt the tribology system and lubrication in hydrogen large-bore engines is investigated, to minimize particle emission. The investigations consider PN with 50% cut-off sizes at 23 nm (PN_{23}) and 10 nm (PN_{10}), whereby influences of the air-fuel equivalence ratio (AFR, analog λ), the indicated mean effective pressure (IMEP), and the relative intake air humidity (RHI) are observed. An extended emission analysis based on the gaseous components total hydrocarbons (THC), CO, and CO_2 further outlines the carbonaceous emissions induced by these oil-based particles.[38,39]

Review

Alrazen *et al.*,[40] Barrios *et al.*,[41] Yang *et al.*,[42] Sharma *et al.*,[43] and Zhou *et al.*[44] investigated particle emissions of hydrogen admixtures in diesel – observing a significant reduction of PM with increasing H_2 admixture rates. Zhao *et al.*[45] discovered similar trends in a Direct Injection (DI) Spark Ignition (SI) engine with a particle emissions decrease of 95% at low loads when blending 10% hydrogen into gasoline. Adding not only hydrogen but CH_4 and CO to diesel by 10% and 20%, Hernández *et al.*[46] also showed the potential to significantly reduce particle emissions by number and mass. Conducting comparable investigations, Singh *et al.*[47,48] analyzed the particle emissions of Port Fuel Injection (PFI) diesel engines operating on diesel, gasoline, compressed natural gas (CNG), hydrogen-enriched CNG, and neat hydrogen. Hydrogen operation thereby showed the lowest particle number emissions with concentrations of 10^6–10^7 # cm^{-3}, slightly increasing with increasing engine load.[47]

Analyzing the particle emissions of a large-bore CNG engine, Ristovski *et al.*[37] stands out as the first and, until now, only publication on particles of CNG large-bore engine operation – investigating not only the particle numbers but also the size distribution with particular interest to the size ranges 15–

700 nm and 50–3000 nm. Further investigations by Distaso *et al.*,[49] Napolitano *et al.*,[50] Toumasatos *et al.*,[51] Dimaratos *et al.*,[52] and Alanen *et al.*[35] were conducted on heavy-duty as well as passenger car vehicles operated on CNG. Alanen *et al.*[35] found the number of particles with a diameter lower than 23 nm to dominate the total particle emission.

Maier *et al.*[53] investigated an automotive-sized DI-SI engine operated on hydrogen and CNG to analyze the fuel-independent particulate emissions. The results showed similar particulate numbers of both gaseous fuels compared to the gasoline reference for particle sizes smaller than 10 nm, whereby particles larger than 30 nm were barely detected with gaseous fuels.[53]

Hora *et al.*[54] investigated particle emission of an SI engine operated on CNG and by 10%, 20%, and 30 vol% hydrogen-enriched CNG at varying engine loads (IMEP). The results showed 30 vol% hydrogen-enriched CNG emitting the highest number of nano-particles amongst the tested HCNG compositions at each engine load – correspondingly leading to higher contributions in size-mass and size-surface area distributions.[54]

In 2007, Miller *et al.*[36] analyzed the influence of lubrication oil on the particle number and size distribution of a CAT3304 four-cylinder diesel engine with a bore of 120 mm by operating it on hydrogen and, therefore, in the absence of fuel-derived soot. The investigations showed particle numbers between 10^5 and 10^7 # cm^{-3} with geometric mean diameters from 18 to 31 nm.[36]

In an interlinked series, Thwako *et al.*[55–58] analyzed the particle emission of engines with bore sizes of 80 and 67 mm operated on natural gas, an H_2–CO_2 reformate (containing 75 mol% H_2 and 25 mol% CO_2), and hydrogen, using an TSI Exhaust Particle Sizer Spectrometer model 3090 and a TSI 379020A-30 Rotating Disk Thermodiluter. A correlation between the particle formation and the engine's load in DI operation was observed.[58] In natural gas operations, the dependency was moderate. For the reformate and hydrogen, a stronger correlation was found, as a sudden increase in particle emission up to 3–4 $\times$ 10^6 # cm^{-3} occurred at higher loads, leading to particle emissions surpassing those of natural gas operation.[55–58] The highest particle emissions were observed in reformate operations due to excessive lubricant participation.[57,58] An earlier performed comparison between the reformate and gasoline showed an almost two times greater particle emission of circa 1 $\times$ 10^8 # cm^{-3} of the DI reformate operation.[55] Comparing DI to PFI for the H_2–CO_2 reformate, PFI resulted in lower particle emissions.[55] By contrasting hydrogen with natural gas in DI operations, an enhanced particle formation was found in hydrogen operation – an increased sighting found within earlier ignition timings. This is suspected to result from hydrogen's low flame quenching distance and the longer jet–wall interaction.[57,58] In summary, the following three aspects were found to affect particle formation: the distance of flame quenching, the content of fuel carbon, and the duration of the jet–wall interaction, showing no effect of the investigated synthetic or mineral lubrication oil.[56–58]

Reconciling with Thwako *et al.*, investigations by Catapano *et al.*[59] on an SI-DI engine with a bore of 72 mm showed high particle emissions of up to 10^7 # cm^{-3} in the size range of 10–50 nm in hydrogen operation.

Berg *et al.*[60] further investigated the influence of load, engine speed, injection timing, AFR, and ignition timing of a DI-SI 90 mm bore hydrogen engine on its particle emissions. Particle numbers and size distributions were measured with a Cambustion DMS 500 fast particle analyzer without a volatile particle remover (VPR).[60] Peak values as high as 5 $\times$ 10^8 # cm^{-3} could be observed for low loads and low intake pressures, most commonly in the 10–30 nm range.[60] Low soot content and, in comparison to diesel particles, high content of organic carbon indicated high involvement of lubrication oil due to a negative pressure gradient from the crankcase to the cylinder during the intake stroke.[60]

Whereas most investigations on particle emissions address different fuel mixes with hydrogen and natural gas, only a few analyze particle emissions of engines solely operated on hydrogen or natural gas in PFI operation and even less on DI design. Research focuses more on passenger car-size engines than large-bore engines, leading to a gap in the state of research regarding large-bore engines operated on hydrogen or natural gas.

Materials and methods

Test bench setup

The experiments for this investigation were conducted on a single-cylinder research engine, based on a series production large-bore gas engine for power generation and railway and marine applications. For engine specifications, see Table 1. The setup allows for thermodynamical investigations of the engine by being equipped with multiple pressure sensors, thermocouples, and piezoresistive sensors in inlet and exhaust manifolds. The test bench setup, in which the engine is embedded, is depicted in Fig. 2. The charge air supply system enables cooled, heated, dry, or saturated charge air with pressures of over 10 bar and a maximum air mass supply of 1000 kg h^{-1}. Saturated steam from softened water is added to the charge air to set the humidity.

For this study, the engine was operated with hydrogen and CNG. The hydrogen is sourced from bundles of 300 bar with a quality of 3.0, whereas the CNG is sourced from the public gas grid, exhibiting an average methane content of 91.52 mol% or 83.01 wt%.[61] The chosen compressed fuel gas is added to the charge air through a venturi mixer. Subsequently, the fuel-air mixture is homogenized before entering the engine. For a more detailed description of the test bench setup, please refer to Armbruster *et al.*[62] As backfire frequently occurs in the SI-PFI engine, for the following hydrogen operation, an unscavenged pre-chamber spark plug with a different electrode material was installed and the intake air temperature was lowered to 30 °C. The compression ratio of 11.65 was kept consistent for all investigations. For lubrication, Sentron LD 8000 by Petro-Canada Lubricants was used in both, hydrogen and natural gas operations. It is a low-ash (0.52 wt%) engine oil with a sulfur content of 0.288 wt%.[63,64]

The exhaust gas line is equipped with temperature and pressure measuring points directly after the outlet ports of the

Table 1 Specifications and operation conditions of the single-cylinder engine

Specifications	Values and details
Bore	170 mm
Stroke	210 mm
Displacement	4.77 l
Components	Series production CNG engine
Compression ratio	11.65
Engine speed	1000–1700 min^{-1}
Valves	2 inlet valves, 2 outlet valves
Valve timing	Light Miller valve timing
Indexing (in-cylinder pressure sensor)	AVL GU21D piezoelectric pressure sensor. Sampling precision of up to 0.05 °CA
Ignition system	Motortech MIC5 (500 mJ prim. energy), unscavenged pre-chamber spark plugs
Injection system	PFI
Start of injection	80 °CA bTDC
Inlet pressure gas	7 bar
Air inlet temperature	30 °C (H_2), 40 °C (CH_4)
Inlet temperature gas	40 °C (H_2), 50 °C (CH_4)
Inlet temperature cooling water	70 °C
Inlet temperature oil	80 °C
Engine oil	Sentron LD 8000
Turbocharger emulation	Exhaust throttle with charger efficiency control
Turbocharger emulator flap	0–50%

cylinder head. Downstream of the measuring points, a Horiba Mexa-ONE D1 and a Horiba Solid Particle Counting System 2300 are connected. The MEXA-ONE D1 measures gaseous emissions, such as CO_2, CO, THC, and NO_x. An exhaust throttle exerts back pressure on the exhaust line upstream simulating the turbocharger efficiency. For studies, the exhaust throttle is generally set to 50% [exhaust throttle position 50% (ETP50)], resulting in an average turbocharger efficiency level of 86%. The throttle position was varied only to investigate a potential influence of the exhaust gas temperature and exhaust backpressure on the particle number.

Particle measurement setup

For counting particle numbers, a Horiba Solid Particle Counting System (SPCS) 2300 was used, consisting of a Condensation Particle Counter (CPC) with a 50% cut-off size at 23 nm. Additionally, a TSI Inc. Model 3772 CPC with a 50% cut-off size at 10 nm was integrated – enabling synchronous measurement. The measurement of nanoparticles is performed by optically enlarging the particles with butanol vapor, which is first condensed and subsequently deposited on the particles. Larger particles are separated through a cyclone-type collector. To ensure butanol condensation, the inlet temperature of the CPCs is set to 40 °C. As volatile material would also condense, a VPR removes such compounds upstream. The VPR is herein designed either as an evaporation tube with a dilution upstream and downstream or as a catalytic stripper (CST) with a dilution upstream. In both cases, the upstream dilution stabilizes the aerosol and intentionally reduces the particle concentration so as not to overload the evaporation tube or CST. This study's particle number measurement system is equipped with a CST, set to a temperature of 350 °C. Detailed information about the setup can be found in the Appendix of Stark *et al.*[65] Contrary to the evaporation tube, the Direct Sampling Unit (DSU) oxidation catalyzer does not only evaporate the material but further prevents re-nucleation by follow-up reactions. This ensures that volatile materials are not mistakenly included in the measurement. The dilution ratios of the first Particle Number Diluter (PND) and DSU are set to 10 and 15. In contrast, the second stage is set to a fixed dilution ratio of 10 – resulting in a total dilution of 1 : 1500. The concentrations given in this study are corrected by this factor and indicate the particle concentration in the exhaust. The particle number counting system is located after the exhaust throttle so as not to be impinged with pressured exhaust gas.

Simulation setup

Computational fluid dynamic (CFD) simulations were conducted to gain insight into the combustion behavior of hydrogen and methane inside the combustion chamber. The CONVERGE[66] software package, version 3.0.25, was utilized as the computational framework. A model of the engine used in the experimental investigations was built using the Reynolds-averaged Navier–Stokes turbulence representation and detailed chemistry calculations to represent the combustion reactions. Following the validation of the charge exchange model using experimental data in motored operation, a model was created for each fuel type to enable a comparative analysis of flame propagation and flame structure. For both fuels, an engine speed of 1500 rpm and an inlet pressure of 2.1 bar were utilized. To be consistent with the experimental operations, an AFR of 2.5 was applied for hydrogen, while for methane, the AFR was set to 1.5. To analyze the near-wall behavior, the propagation of OH radicals, which indicate the flame front, was investigated to determine the distance of the flame to the wall throughout the combustion process.

Test procedure

Particle measurements were performed at varying AFR, IMEP, and RHI successively for both hydrogen and CNG operations

while maintaining identical injection conditions. These included an engine speed of 1500 rpm, and a specific center of combustion (CoC) value, which is defined as the degree of crank angle at 50% of burnt fuel mass. The CoC was optimized for each fuel to ensure stable combustion. The calculated AFR varied from 1.4 to 1.7 in steps of 0.05 for CNG and from 2.5 to 2.9 in steps of 0.10 for hydrogen while maintaining an IMEP of 16.5 bar for CNG and 15 bar for hydrogen operation at a constant RHI of 0%. The CoC was kept constant at 16 °CA aTDC (crank angle degree after top dead center) for CNG and at 10 °CA aTDC for hydrogen operation by varying the ignition timing. For IMEP variations, the AFR was kept at a constant 1.6 for CNG and 2.5 for hydrogen operation at an RHI of 0%. The IMEP was varied from 16 to 21 bar in steps of 1 bar for CNG operation and from 15 to 17 bar in steps of 0.5 bar for hydrogen operation. While varying the RHI from 0 to 80% in steps of 20%, the AFR and IMEP were kept at a constant 1.6 and 17.5 bar for CNG operation and 2.5 and 16 bar for hydrogen operation. The elevated load in natural gas operation results from operating on a consistently low compression ratio of 11.65 – optimized for hydrogen operation – necessitating a higher load level to ensure stable natural gas combustion. The criterion for stable combustion is a standard deviation σ of the IMEP of less than 3.

In addition to a fired operation, particle measurements of the inlet and exhaust air were also conducted in the motored operation. Therefore, the intake air was supercharged at 1, 2, and 4 bar, the RHI was varied from 0% to saturation in steps of 20%, and the engine speed in three steps from 1000 to 1750 rpm. To rule out relations, additional experiments were conducted with an open exhaust throttle (ETP0) – reducing the exhaust gas temperature due to a lower resulting back pressure.

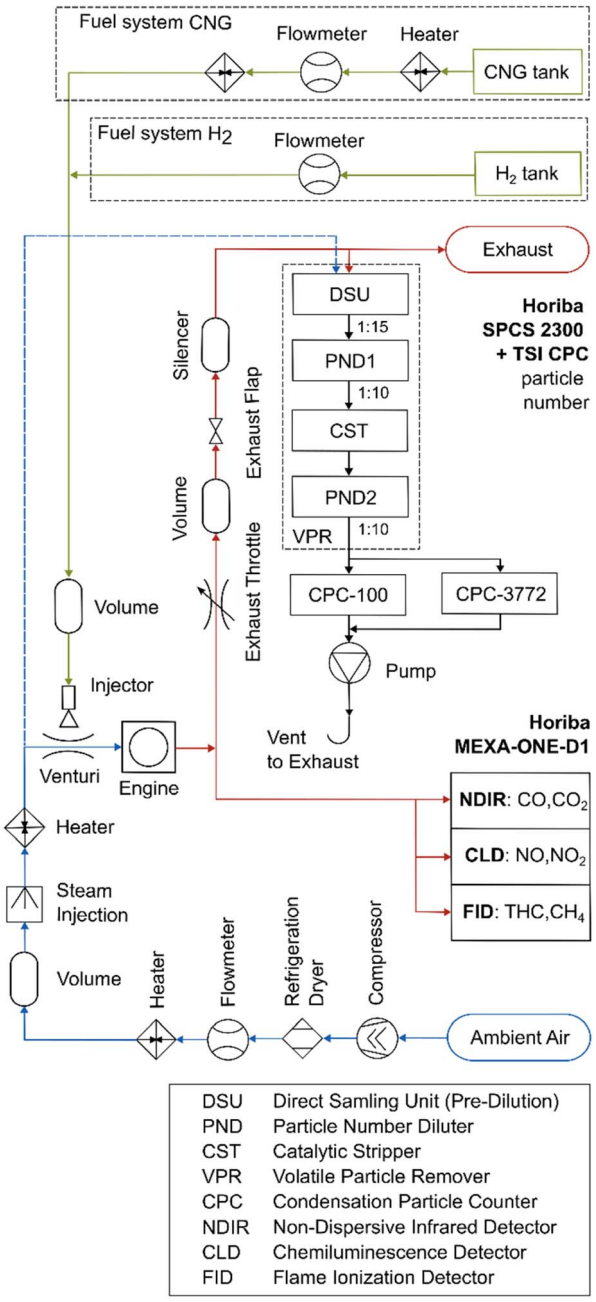

Fig. 2 Overview of the test bench and particle measurement setup with the two successively used sampling points in the intake and exhaust line.

Results and discussion

For comparison to the background concentration, PN was not only measured in the exhaust but also in the intake air, compare Fig. 3 and 4. Results for the intake air are consistently close to zero (<1000 # cm^{-3}) and are thus assumed to be negligible. With particle formation from intake air pollution and fuel influence being ruled out, particle emissions can only be led back to lubrication oil contribution and metallic abrasion. The

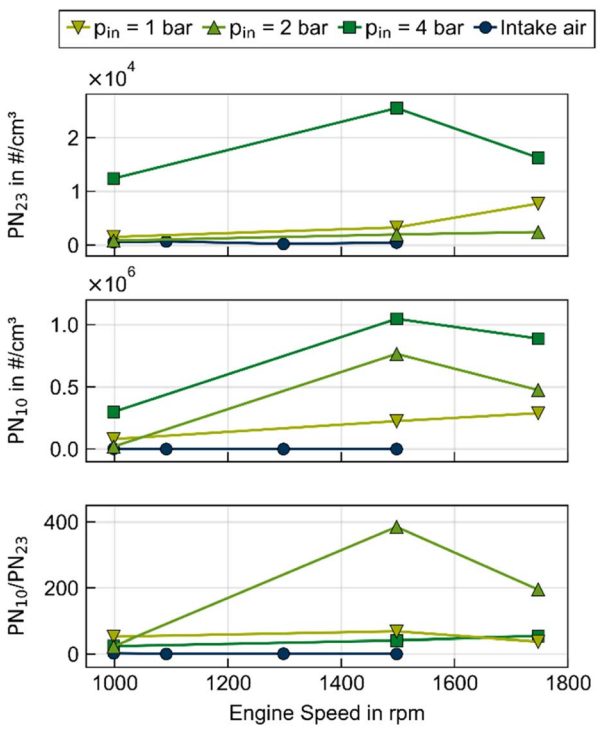

Fig. 3 PN_{23}, PN_{10}, and PN_{10}/PN_{23} ratio in motored operation with additional PN in intake air for variations of the engine speed and the engine's supercharging level, defined as p_{in}.

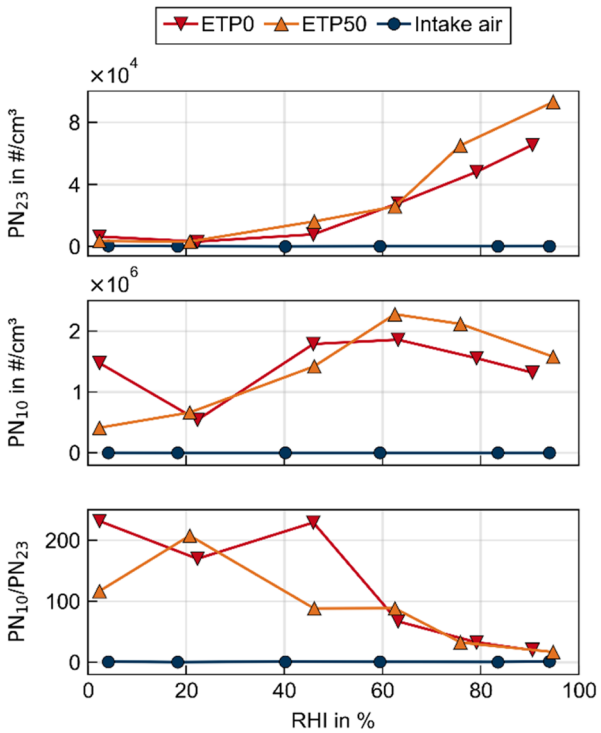

Fig. 4 PN_{23}, PN_{10}, and PN_{10}/PN_{23} ratio in motored operation with additional PN in intake air for variations of the relative humidity in the intake and the exhaust throttle position.

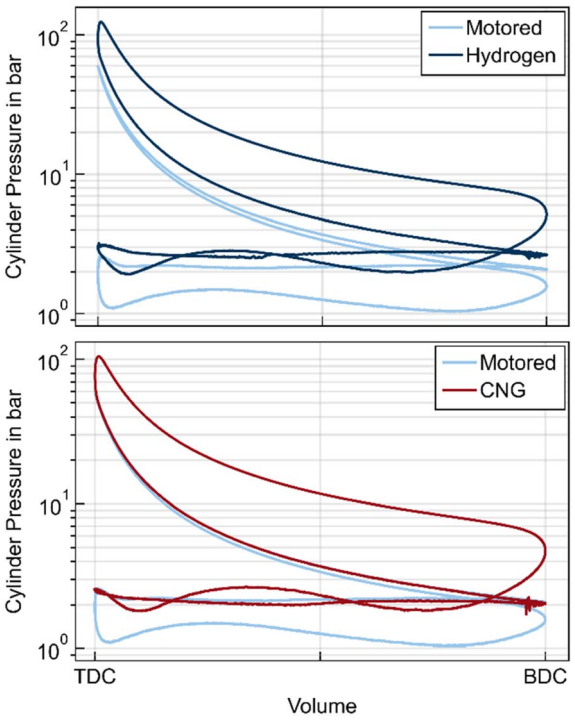

Fig. 5 p–v diagram operated on hydrogen at 1500 rpm, AFR = 2.5, 16 bar IMEP, and operated on CNG at 1500 rpm, AFR = 1.6, 16 bar IMEP compared to motored operation.

lubrication oil was kept consistent over all operations, motored and fired for both, hydrogen and natural gas operations.

The covariation of motored operation in Fig. 3 shows the influence of the engine speed and the engine's supercharging level, defined as the intake pressure (p_{in}), on PN measured in the exhaust line. With higher engine speeds, PN_{23} and PN_{10} rise. Likewise, both rise with higher supercharging up to 10^4 # cm^{-3} for PN_{23} and 10^5 # cm^{-3} for PN_{10}, suggesting a maximum of lubrication oil involvement for the highest set supercharging level at the conventional engine speed of 1500 rpm. Additionally, the engine speed has a major impact on piston and piston ring friction, which leads to metallic abrasion and, therefore, particle emissions based on engine wear.

Fig. 4 shows the influence of the RHI and the exhaust throttle position, varying the exhaust backpressure and temperature, on the particle emission. At RHI's of over 45%, PN exceeds such of covariation in Fig. 3, resulting in a maximum of 2.27×10^6 # cm^{-3} at 60% RHI for PN_{10} and of 9.31×10^4 # cm^{-3} at 95% RHI for PN_{23}. With higher RHI, PN_{10} decreases again while PN_{23} increases, which is also observable by the decreasing ratio of PN_{10}/PN_{23}. This leads to the assumption of agglomeration processes. Minimizing exhaust backpressure thereby tends to slightly lower PN. The results indicate that the lubrication oil at the liner surface is more likely to be carried away with greater in-cylinder pressure during the intake stroke and lower pressure during the exhaust stroke. Operating the engine with a Miller valve timing and lowering the in-cylinder pressure and temperature by closing the intake valve before the top dead center is also assumed to encourage particle formation. In Fig. 5 and 6, the in-cylinder pressure over the in-cylinder volume and the crank angle degree in hydrogen and CNG operation are compared to the motored operation. During the fired operation, the pressure rises to approximately 119 bar during CNG operation and 128 bar during hydrogen operation in IMEP variation. In contrast, the maximum pressure by compression only results in approximately 60 bar (see Fig. 6). Hydrogen's higher flame speed leads to a higher maximum pressure compared to natural gas, despite the lower IMEPs.

An overview of the variations in fired operation is given in Table 2. The results are shown in Fig. 7. Analyzing the fired operation, a correlation between PN_{23} and PN_{10} emission and RHI is not evident for either hydrogen or natural gas. Consequently, the ratio between PN_{23} and PN_{10} remains constant. This indicates that a slight increase in the heat capacity of moist intake air compared to dry intake air has no noticeable effect on the number of particles. Furthermore, this also confirms the CST's ability to remove volatile particles. The variation in AFR conversely affects particle emissions in both operations, increasing PN_{23} and PN_{10} with leaner combustion. This effect is slightly more pronounced for smaller particles in both hydrogen and natural gas operations, resulting in a higher PN_{10}/PN_{23} ratio. The correlation between AFR and particulate matter cannot be solely attributed to fuel combustion, as the effect is observed in both natural gas and hydrogen engines, with the latter having no combustion-induced particle emissions. This suggests that oil-induced particles are influenced by in-cylinder temperature, with higher temperatures resulting in

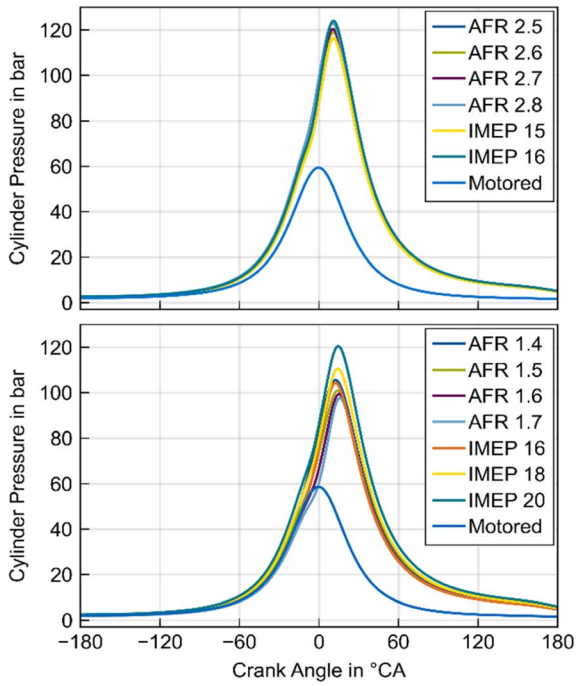

Fig. 6 Cylinder pressure trace for variations of AFR and IMEP in CNG, hydrogen, and motored operation at 1500 rpm.

fewer PN_{23} and PN_{10}, and PN_{10} being more affected by temperature. However, this hypothesis requires further investigation.

The tendency of lower PN with ETP0 is also observable in natural gas operation, analogous to motored operation, resulting in an average PN reduction of 21.6% for PN_{23} and 24.1% for PN_{10} in comparison to ETP50. This may be related to the dependence of the exhaust back pressure on in-cylinder flow conditions during load exchange, which can lead to varying oil wall detachment processes, resulting in different levels of particulate formation.

The knowledge found in OME operation can be transferred while measuring particles in natural gas operation: with a lack of intramolecular C–C-bonds, the agglomeration of soot stemming from the fuel combusting is greatly inhibited.[15,18,19] This results in particle emissions lower than 2×10^4 # cm^{-3} regarding PN_{23} and lower than 4×10^4 # cm^{-3} regarding PN_{10} over all investigations. Hydrogen operation, meanwhile, results in particle emissions lower than 8×10^4 # cm^{-3} regarding PN_{23} and a maximum of 1.5×10^5 # cm^{-3} regarding PN_{10}, occurring at the lowest maximum in-cylinder pressure at an IMEP of 15 bar. The overall higher particle numbers in motored operation likely stem from the difference in in-cylinder pressure during the combustion stroke, reducing lubrication oil detachment.

The composition of the particles was not analyzed as part of this publication. Therefore, it is not possible at this stage to make any statements about the impact of the particles on the environment and health. Analyzing the particle composition would also provide insights into the particle mass.

In engines where particles are both oil- and fuel-induced, as is the case in diesel engines, particles in the range of 30 to 120 nm and larger are increasingly found in the raw exhaust.[24,46,67,68] A similar particle density in hydrogen and CNG engines would result in a relatively low total particle mass for the particle sizes present.

The shift towards smaller particle sizes in hydrogen and CNG engines suggests that oil-dependent particles may agglomerate with fuel-dependent particles in conventionally fueled engines – forming larger particles in the process. To further investigate this presumption, *in situ* gas sampling at different crank angles could be conducted, as presented in Pflaum *et al.*[69]

The slightly increased particle numbers in hydrogen operation in comparison to natural gas are assumed to result from the increased lubricating oil influence due to the hydrogen's combustion closer to the combustion chamber wall,[70–72] leading to particle emissions of ash originating from this oil. As depicted in Fig. 9, simulation results confirm that hydrogen has a lower flame-quenching distance than methane. Furthermore, the simulations show that the hydrogen–air mixture spreads more rapidly within the cylinder. This leads to an earlier and longer flame–wall interaction in hydrogen operation compared to methane operation.

In addition, the pre-mixed combustion process is assumed to lead to hydrogenation of the lubricating oil. This might lead to additional particle formation. The interaction of fuel and lubricating oil is more pronounced in DI operation – depending on spray breakup and injector position.

To evaluate the carbonaceous impact of the lubricating oil combustion, leading to particle emissions, Fig. 8 presents THC, CO, and CO_2 emissions across variations of AFR, IMEP, and RHI in ppm for both natural gas and hydrogen operation. Contrary to natural gas operation, the carbonaceous emissions concentrations in hydrogen operation are below the detection limit of the measuring instruments used – resulting in indicated values of 0 ± 0.5 ppm for CO concentration and 0 ± 6 ppm for THC concentration. A minimum of 500 ppm CO_2 emission likely

Table 2 Overview of variations conducted in fired engine operation

Variation		AFR (step size) in —	IMEP (step size) in bar	RHI (step size) in %
AFR	H_2	2.5–2.9 (0.10)	15	0
	CNG	1.4–1.7 (0.05)	16.5	0
IMEP	H_2	2.5	15–17 (0.5)	0
	CNG	1.6	16–21 (1)	0
RHI	H_2	2.5	16	0–80 (20)
	CNG	1.6	17.5	0–80 (20)

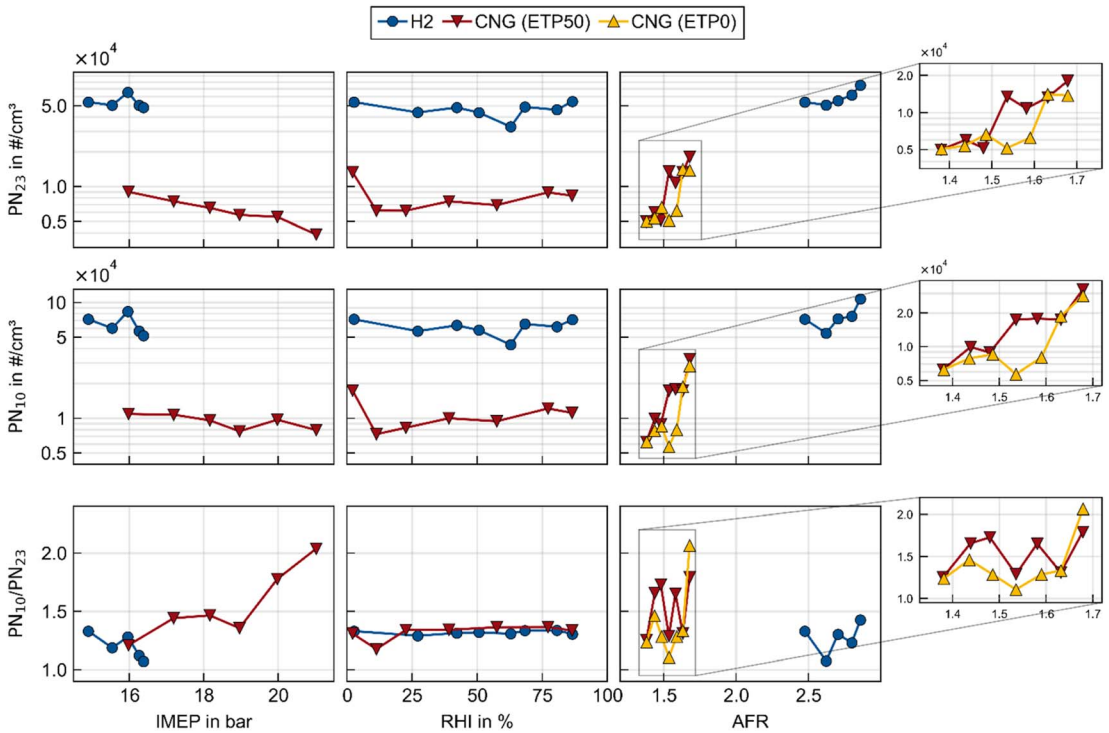

Fig. 7 PN_{23}, PN_{10}, and PN_{10}/PN_{23} ratio in hydrogen and natural gas operations for variations of AFR, IMEP, and the relative humidity in the intake, additionally varying the exhaust throttle position in natural gas operation.

arises due to the CO_2 concentration in the intake air.[73] The values shown in Fig. 8 represent the total measured emissions, including the baseline CO_2 concentration from the intake air. In natural gas operations, THC emissions rise with increasing AFR due to more incomplete combustion. A closer look at emissions of THC is taken by Armbruster *et al.*,[62] proving CH_4 to be the predominant contributor to THC in natural gas operations.

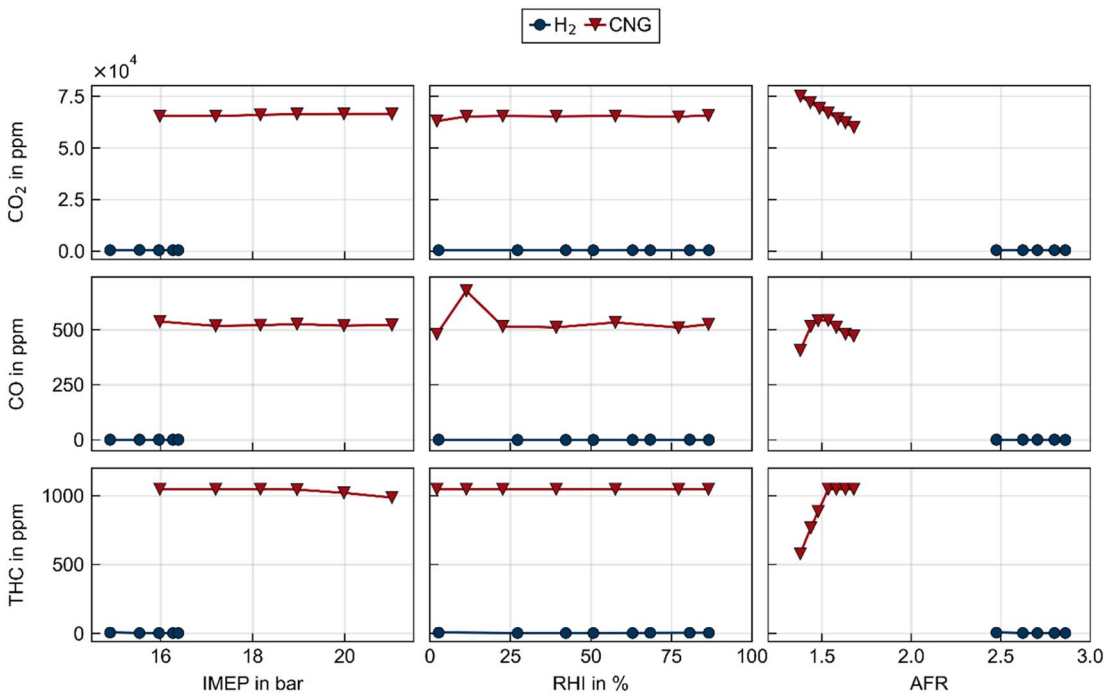

Fig. 8 Absolute CO_2, CO, and THC emissions in hydrogen and natural gas operations for variations of AFR, IMEP, and the relative humidity in the intake.

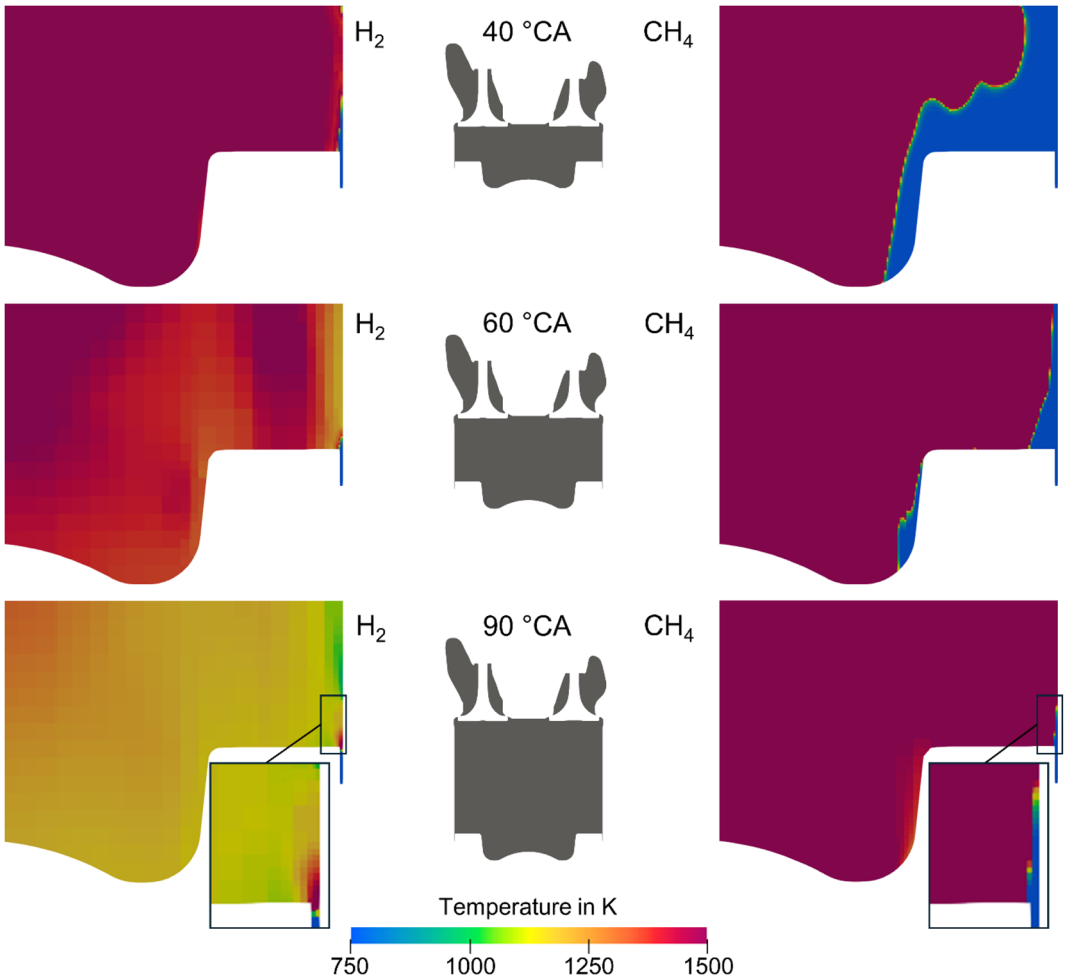

Fig. 9 3D CFD simulations of hydrogen and methane combustion at an AFR = 2.5 for hydrogen operation and an AFR = 1.5 for methane operation at 1500 rpm, comparing flame propagation and flame quenching distance for 40 °CA, 60 °CA and 90 °CA after TDC.

Through higher RHI and, therefore, higher heat capacity in the intake air, the combustion speed slows down, and maximum combustion temperatures are reduced, enabling a higher knocking resistance. However, invariably concomitant with higher RHI is a reduction of the engine efficiency. With an average of 47.9%, the engine's indicated efficiency η_i in hydrogen operation tops such of natural gas operation with an average of 43.2%, justified in hydrogen's combustion behavior.[3,4,61,74] Similar results were observed in Armbruster *et al.*,[62] Eicheldinger *et al.*,[75] and Peters *et al.*[76]

Conclusion and outlook

Analyzing the previous state of research, trends in investigating the particulate emissions of automotive or heavy-duty engines being partly or solely operated on natural gas or hydrogen can be noticed as both fuels gain attractiveness due to their potential for global decarbonization. Blends of both fuels with gasoline and diesel are known to have the potential to drastically reduce particle emissions. Natural gas- and hydrogen-powered PFI engines also enable engine operations with reduced pollutant emissions. Regarding particle emissions, most PN results from fuel-independent particle emissions, *e.g.*, ash originating from lubricating oil and engine wear. Investigating a large SI-PFI engine operated on hydrogen and natural gas for the first time in this study and the results found in automotive and heavy-duty engines can be confirmed: particle emissions measured down to 10 nm amount up to 10^4–10^5 # cm^{-3}, whereby particle introduction due to the intake air was ruled out. Unexpectedly, PN emissions from hydrogen operations are slightly higher than those of natural gas operations. This is assumed to result from the increased lubricating oil influence due to hydrogen's reduced quenching distance to the combustion chamber wall and interaction with the oil film. It may be worthwhile to examine the tribological components, *e.g.*, piston rings and piston design for hydrogen engines due to the stated differences. However, the results indicate no significant relevance concerning the regulated emission limit values. The particulate emission of the motored operation of the charged engine surpasses the fired operation. The particle count also rises with higher charging and engine speed, influencing the contribution of lubrication oil. Still, an extended emissions analysis based on the gaseous components THC, CO, and CO_2 shows negligible carbonaceous emissions in hydrogen operation.

Consequent to developments in hydrogen engines, specifically their injection concepts, research on particulate emissions lately tends towards hydrogen DI-engines. The results thereby show particle emissions like such of long-chain hydrocarbon fuels for nanosize particles, likely stemming from lubrication oil. Therefore, this study's findings are planned to be compared with the results of a DI setup of the single-cylinder research engine in the future. Furthermore, investigating PN emissions in hydrogen-powered HPDF engines with OME as pilot fuel is of great interest.[77] Investigations on the particle composition and *in situ* gas sampling would additionally support the research on fuel-independent particles.

Abbreviations

AFR	Air–fuel ratio (lambda)
BDC	Bottom dead center
aTDC	After top dead center
bTDC	Before top dead center
CFD	Computational fluid dynamics
CLD	Chemiluminescence detector
CNG	Compressed natural gas
CoC	Center of combustion
CPC	Condensation particle counter
CST	Catalytic stripper
DI	Direct injection
DSU	Direct sampling unit
EOI	End of injection
FID	Flame ionization detector
FTIR	Fourier-transform infrared spectroscopy
HCNG	Hydrogen-enriched CNG
ICE	Internal combustion engine
IMEP	Indicated mean effective pressure
mol%	Percentage by mole
NDIR	Non-dispersive infrared detectors
OME	Oxymethylene ether
PFI	Port fuel injection
p_{in}	Intake air pressure (supercharging level)
PM	Particle mass
PN	Particle number emission
PN_{10}	Particle number emission with a 50% cut-off at 10 nm
PN_{23}	Particle number emission with a 50% cut-off at 23 nm
PND	Particle number diluter
PPM	Parts per million
PtG	Power to gas
RHI	Relative humidity intake
RPM	Revolutions per minute
SCE	Single-cylinder engine
SI	Spark ignited
SOI	Start of injection
SPCS	Solid particle counting system
TA	Technical instructions on clean air
TDC	Top dead center
THC	Total hydrocarbons
TUM	Technical University of Munich
vol%	Percentage by volume
VPR	Volatile particle remover
wt%	Percentage by mass
30HCNG	Hydrogen-enriched CNG by 30 vol% hydrogen
°C	Degree Celsius
°CA	Crank angle degree

Data availability

The data supporting this article have been included as part of the ESI.†

Author contributions

Felina Armbruster: conceptualization, experimental setup, data curation (experimental), formal analysis, investigation, methodology, project administration, software, validation, visualization, writing – original draft, writing – review & editing. Alexander Gelner: conceptualization, formal analysis, validation, methodology, writing – original draft, writing – review & editing. Andreas Zepf: investigation, software, simulation setup, data curation (simulation), visualization, writing – review & editing. Maximilian Prager: funding acquisition, project administration, supervision, writing – review & editing. Martin Härtl: conceptualization, funding acquisition, project administration, supervision, writing – review & editing. Malte Jaensch: funding acquisition, project administration, supervision, writing – review & editing.

Conflicts of interest

The authors declare that they have no known competing financial interests or personal relationships that could have appeared to influence the work reports in this paper.

Acknowledgements

The authors thank Catalytic Instruments GmbH & Co. KG for providing a Catalytic Stripper and technical support. Convergent Science provided CONVERGE licenses and technical support for this work.

Notes and references

1 United Nations, *The Sustainable Development Goals Report 2023. Special Edition*, Department of Economic and Social Affairs, 2023, accessed 2 May 2024.
2 United Nations, *Sustainable Development Goals*, accessed 2 May 2024.
3 *Zukünftige Kraftstoffe*, ed. W. Maus, Springer Berlin Heidelberg, Berlin, Heidelberg, 2019.
4 W. J. Nuttall and A. T. Bakenne, *Fossil Fuel Hydrogen*, Springer International Publishing, Cham, 2020.
5 Bundesumweltamt, *Emissionen des Verkehrs*, **https://www.umweltbundesamt.de/daten/verkehr/emissionen-des-verkehrs#verkehr-belastet-luft-und-klima-minderungsziele-der-bundesregierung**, accessed 18 August 2023.
6 United States Environmental Protection Agency (EPA), *Greenhouse Gas Emissions*, **https://www.epa.gov/**

ghgemissions/sources-greenhouse-gas-emissions, accessed 10 May 2024.
7 European Environment Agency (EEA), *Sector Share of Nitrogen Oxides Emissions*, https://www.eea.europa.eu/data-and-maps/daviz/sector-share-of-nitrogen-oxides-emissions#tab-chart_1, accessed 10 May 2024.
8 European Environment Agency (EEA), *Sector Share for Emissions of Primary PM2.5 and PM10 Particulate Matter*, https://www.eea.europa.eu/data-and-maps/daviz/sector-split-of-emissions-of-4#tab-chart_1, accessed 10 May 2024.
9 C. J. L. Murray, A. Y. Aravkin, P. Zheng, C. Abbafati, *et al.*, Global burden of 87 risk factors in 204 countries and territories, 1990-2019: a systematic analysis for the Global Burden of Disease Study 2019, *Lancet*, 2020, **396**, 1223–1249.
10 I. Kheirbek, J. Haney, S. Douglas, K. Ito and T. Matte, The contribution of motor vehicle emissions to ambient fine particulate matter public health impacts in New York City: a health burden assessment, *Environ. Health*, 2016, **15**, 89.
11 T. J. Grahame and R. B. Schlesinger, Cardiovascular health and particulate vehicular emissions: a critical evaluation of the evidence, *Air Qual., Atmos. Health*, 2010, **3**, 3–27.
12 T. C. Bond, S. J. Doherty, P. M. Forster, *et al.*, Bounding the role of black carbon in the climate system: A scientific assessment, *J. Geophys. Res.: Atmos.*, 2013, **118**, 5380–5552.
13 *Clean Air Act: A Summary of the Act and its Major Requirements*, ed. Congressional Research Service, 2022, updated September 13, 2022.
14 B. Giechaskiel, A. Melas, G. Martini and P. Dilara, Overview of Vehicle Exhaust Particle Number Regulations, *Processes*, 2021, **9**, 2216.
15 M. Härtl, P. Seidenspinner, G. Wachtmeister and E. Jacob, Synthetic Diesel Fuel OME1 A Pathway Out of the Soot-NOx Trade-Off, *MTZ Worldwide*, 2014, **75**, 48–53.
16 P. Dworschak, V. Berger, M. Härtl and G. Wachtmeister, Particle Size Distribution Measurements of Neat and Water-Emulsified Oxymethylene Ethers in a Heavy-Duty Diesel Engine, *SAE Int. J. Fuels Lubr.*, 2020, **13**(2), 187–203.
17 S. Blochum, F. Fellner, M. Mühlthaler, M. Härtl, G. Wachtmeister, N. Yoneya and H. Sauerland, in *SAE Technical Paper Series*, SAE International, 400 Commonwealth Drive, Warrendale, PA, United States, 2021.
18 A. D. Gelner, G. A. Pang, M. Weber, C. Haisch, H. A. Beck, C. Pastoetter, M. Härtl, M. Jaensch and G. Wachtmeister, Gaseous emissions of a heavy-duty engine fueled with polyoxymethylene dimethyl ethers (OME) in transient cold-start operation and methods for after-treatment system heating, *Environ. Sci.: Adv.*, 2022, **1**, 470–482.
19 A. D. Gelner, D. Rothe, C. Kykal, M. Irwin, A. Sommer, C. Pastoetter, M. Härtl, M. Jaensch and G. Wachtmeister, Particle emissions of a heavy-duty engine fueled with polyoxymethylene dimethyl ethers (OME), *Environ. Sci.: Atmos.*, 2022, **2**, 291–304.
20 S. E. Iannuzzi, C. Barro, K. Boulouchos and J. Burger, Combustion behavior and soot formation/oxidation of oxygenated fuels in a cylindrical constant volume chamber, *Fuel*, 2016, **167**, 49–59.
21 M. Zubel, T. Ottenwälder, B. Lehrheuer, S. Pischinger, K. Gaukel, D. Pelerin, M. Härtl and G. Wachtmeister, *XME-Diesel. (Bio-)Methylether als alternative Kraftstoffe in bivalenten Diesel-Brennverfahren*, Final Report, 2019.
22 H. Burtscher, Physical characterization of particulate emissions from diesel engines: a review, *J. Aerosol Sci.*, 2005, **36**, 896–932.
23 A. A. Salvi, D. Assanis and Z. Filipi, Impact of Physical and Chemical Properties of Alternative Fuels on Combustion, Gaseous Emissions, and Particulate Matter during Steady and Transient Engine Operation, *Energy Fuels*, 2012, **26**, 4231–4241.
24 K. Yehliu, A. L. Boehman and O. Armas, Emissions from different alternative diesel fuels operating with single and split fuel injection, *Fuel*, 2010, **89**, 423–437.
25 R. K. Singh, A. Sarkar and J. P. Chakraborty, Influence of Alternate Fuels on the Performance and Emission from Internal Combustion Engines and Soot Particle Collection Using Thermophoretic Sampler: A Comprehensive Review, *Waste Biomass Valorization*, 2018, **10**, 2801–2823.
26 S. M. Ramírez Pérez, *Euro 7 Motor Vehicle Emission Standards*, https://www.europarl.europa.eu/RegData/etudes/ATAG/2023/754573/EPRS_ATA(2023)754573_DE.pdf, accessed 7 June 2024.
27 S. Schemme, R. C. Samsun, R. Peters and D. Stolten, Power-to-fuel as a key to sustainable transport systems – An analysis of diesel fuels produced from CO_2 and renewable electricity, *Fuel*, 2017, **205**, 198–221.
28 C. Wulf, J. Linßen and P. Zapp, Review of Power-to-Gas Projects in Europe, *Energy Procedia*, 2018, **155**, 367–378.
29 Bundesministerium für Ernährung und Landwirtschaft, *Klimaschutzprogramm 2030. Klimaschutzprogramm 2030 der Bundesregierung zur Umsetzung des Klimaschutzplans 2050*, 2019, https://www.bmel.de/SharedDocs/Downloads/DE/_Landwirtschaft/Klimaschutz/Klimaschutzprogramm2030.html, accessed 27 December 2023.
30 Bundesministerium für Umwelt, Naturschutz, Bau und Reaktorsicherheit (BMUB), *Kurzinformationen Elektromobilität bezüglich Strom- und Ressourcenbedarf*, https://www.bmuv.de/fileadmin/Daten_BMU/Download_PDF/Verkehr/emob_strom_ressourcen_bf.pdf, accessed 27 December 2023.
31 G. Pirker and A. Wimmer, Sustainable power generation with large gas engines, *Energy Convers. Manage.*, 2017, **149**, 1048–1065.
32 Bundesregierung, *Die Nationale Wasserstoffstrategie*, https://www.bmwk.de/Redaktion/DE/Pressemitteilungen/2020/20200610-globale-fuehrungsrolle-bei-wasserstofftechnologien-sichern.html#:~:text=Einleitung.%20%C2%A9%20BMWi%2FAndreas%20Mertens.%20Das%20Bundeskabinett%20hat%20heute,sich%20Wasserstofftechnologien%20zu%20einem%20zentralen%20Gesch%C3%A4ftsfeld%20der%20?msclkid=90f4cbc4c14811ec9f31338c554750ce, accessed 21 April 2022.

33 Bundesministerium für Umwelt und Klimaschutz, *Erdgasversorgung in Deutschland*, **https://www.bmwk.de/Redaktion/DE/Artikel/Energie/gas-erdgasversorgung-in-deutschland.html**, accessed 20 December 2023.
34 A. Ratzke, PhD thesis, Gottfried Wilhelm Leibniz Universität Hannover, 2013.
35 J. Alanen, E. Saukko, K. Lehtoranta, T. Murtonen, H. Timonen, R. Hillamo, P. Karjalainen, H. Kuuluvainen, J. Harra, J. Keskinen and T. Rönkkö, The formation and physical properties of the particle emissions from a natural gas engine, *Fuel*, 2015, **162**, 155–161.
36 A. L. Miller, C. B. Stipe, M. C. Habjan and G. G. Ahlstrand, Role of lubrication oil in particulate emissions from a hydrogen-powered internal combustion engine, *Environ. Sci. Technol.*, 2007, **41**, 6828–6835.
37 Z. D. Ristovski, L. Morawska, J. Hitchins, S. Thomas, C. Greenaway and D. Gilbert, Particle Emissions from Compressed Natural Gas Engines, *J. Aerosol Sci.*, 2000, **31**, 403–413.
38 S. Roiser, P. Christoforetti, E. Schutting and H. Eichlseder, Emission behaviour and after treatment of stationary and transient operated hydrogen engines, *Int. J. Engine Res.*, 2023, 146808742311723.
39 *Grundlagen Verbrennungsmotoren. Funnktionsweise und alternative Antriebssysteme Verbrennung, Messtechnik und Simulation*, ed. G. P. Merker and R. Teichmann, Springer Fachmedien Wiesbaden, Wiesbaden, 2019.
40 H. A. Alrazen, A. R. Abu Talib, R. Adnan and K. A. Ahmad, A review of the effect of hydrogen addition on the performance and emissions of the compression – Ignition engine, *Renewable Sustainable Energy Rev.*, 2016, **54**, 785–796.
41 C. C. Barrios, A. Domínguez-Sáez and D. Hormigo, Influence of hydrogen addition on combustion characteristics and particle number and size distribution emissions of a TDI diesel engine, *Fuel*, 2017, **199**, 162–168.
42 Z. Yang, C. Chu, L. Wang and Y. Huang, Effects of H_2 addition on combustion and exhaust emissions in a diesel engine, *Fuel*, 2015, **139**, 190–197.
43 P. Sharma and A. Dhar, Effect of hydrogen supplementation on engine performance and emissions, *Int. J. Hydrogen Energy*, 2018, **43**, 7570–7580.
44 J. H. Zhou, C. S. Cheung and C. W. Leung, Combustion, performance, regulated and unregulated emissions of a diesel engine with hydrogen addition, *Appl. Energy*, 2014, **126**, 1–12.
45 H. Zhao, R. Stone and L. Zhou, Analysis of the particulate emissions and combustion performance of a direct injection spark ignition engine using hydrogen and gasoline mixtures, *Int. J. Hydrogen Energy*, 2010, **35**, 4676–4686.
46 J. J. Hernández, M. Lapuerta and J. Barba, Separate effect of H_2, CH_4 and CO on diesel engine performance and emissions under partial diesel fuel replacement, *Fuel*, 2016, **165**, 173–184.
47 A. P. Singh, A. Pal and A. K. Agarwal, Comparative particulate characteristics of hydrogen, CNG, HCNG, gasoline and diesel fueled engines, *Fuel*, 2016, **185**, 491–499.
48 A. P. Singh, A. Pal, N. K. Gupta and A. K. Agarwal, Particulate emissions from laser ignited and spark ignited hydrogen fueled engines, *Int. J. Hydrogen Energy*, 2017, **42**, 15956–15965.
49 E. Distaso, R. Amirante, P. Tamburrano and R. D. Reitz, Steady-state Characterization of Particle Number Emissions from a Heavy-Duty Euro VI Engine Fueled with Compressed Natural Gas, *Energy Procedia*, 2018, **148**, 671–678.
50 P. Napolitano, M. Alfè, C. Guido, V. Gargiulo, V. Fraioli and C. Beatrice, Particle emissions from a HD SI gas engine fueled with LPG and CNG, *Fuel*, 2020, **269**, 117439.
51 Z. Toumasatos, A. Kontses, S. Doulgeris, Z. Samaras and L. Ntziachristos, Particle emissions measurements on CNG vehicles focusing on Sub-23 nm, *Aerosol Sci. Technol.*, 2021, **55**, 182–193.
52 A. Dimaratos, Z. Toumasatos, G. Triantafyllopoulos, A. Kontses and Z. Samaras, Real-world gaseous and particle emissions of a Bi-fuel gasoline/CNG Euro 6 passenger car, *Transport. Res. D: Transport Environ.*, 2020, **82**, 102307.
53 A. Maier, U. Klaus, A. Dreizler and H. Rottengruber, Fuel-Independent Particulate Emissions in an SIDI Engine, *SAE Int. J. Engines*, 2015, **8**, 1334–1341.
54 T. S. Hora, P. C. Shukla and A. K. Agarwal, Particulate emissions from hydrogen enriched compressed natural gas engine, *Fuel*, 2016, **166**, 574–580.
55 A. Thawko, H. Yadav, A. Eyal, M. Shapiro and L. Tartakovsky, Particle emissions of direct injection internal combustion engine fed with a hydrogen-rich reformate, *Int. J. Hydrogen Energy*, 2019, **44**, 28342–28356.
56 A. Thawko, H. Yadav, M. Shapiro and L. Tartakovsky, in *SAE Technical Paper Series*, SAE International, 400 Commonwealth Drive, Warrendale, PA, United States, 2020.
57 A. Thawko and L. Tartakovsky, The Mechanism of Particle Formation in Non-Premixed Hydrogen Combustion in a Direct-Injection Internal Combustion Engine, *Fuel*, 2022, **327**, 125187.
58 A. Thawko, A. Eyal and L. Tartakovsky, Experimental comparison of performance and emissions of a direct-injection engine fed with alternative gaseous fuels, *Energy Convers. Manage.*, 2022, **251**, 114988.
59 F. Catapano, S. Di Iorio, A. Magno, P. Sementa and B. M. Vaglieco, A Complete Assessment of the Emission Performance of an SI Engine Fueled with Methanol, Methane and Hydrogen, *Energies*, 2024, **17**, 1026.
60 V. Berg, L. Koopmans, J. Sjöblom and P. Dahlander, in *2023 JSAE/SAE Powertrains Japan*, 2023.
61 SWM Service GmbH, *Erdgasbeschaffenheit im Erdgasnetz der SWM Infrastruktur GmbH & CO. KG Oktober 2023*, Laboar/TS-TQ-AP, 2023.
62 F. Armbruster, C. Kraus, M. Prager, M. Härtl and M. Jaensch, Optimized Emission Analysis in Hydrogen Internal Combustion Engines: Fourier Transform Infrared Spectroscopy Innovations and Exhaust Humidity Analysis, *SAE Int. J. Engines*, 2024, **27**(7), 1–17.

63 Liquon Schmierstoff GmbH, *Sentron LD 8000: Premium Motorenöl für stationäre Gasmotoren*, 2022, **https://www.liquon.com/petro-canada-sentron-ld-8000/15017880**.
64 Liquon Schmierstoff GmbH, *Sentron: Motorenöle für stationäre Gasmotoren*, **https://www.liquon.com/petro-canada-sentron-ld-8000/15017880**, accessed 3 June 2024.
65 M. Stark, C. Kraus, F. Fellner and M. Jaensch, Combined exhaust gas and optical investigation of methanol DI-engine with focus on the fuel spray-wall interaction, *Int. J. Engine Res.*, 2024, 1–17.
66 K. J. Richards, P. K. Senecal and E. Pomraning, *CONVERGE 3.0*, Convergent Science, Madison, WI, 2024.
67 G. Lepperhoff, Influences on the Particle Size Distribution of Diesel Particulate Emissions, *Top. Catal.*, 2001, **16/17**, 249–254.
68 A. Sarvi, J. Lyyränen, J. Jokiniemi and R. Zevenhoven, Particulate emissions from large-scale medium-speed diesel engines: 1. Particle size distribution, *Fuel Process. Technol.*, 2011, **92**, 1855–1861.
69 S. Pflaum, A. Heubuch and G. Wachtmeister, Gasentnahmesonde zur zeitlich hoch aufgelösten Entnahme von Brennraumproben, *Motortech. Z.*, 2009, **70**, 868–877.
70 N. Beishuizen, D. Mayer and D. Efimov, *Quenching and flash-back of hydrogen flames on perforated plate burners*, **https://www.researchgate.net/profile/Nijso-Beishuizen/publication/336891194_Quenching_and_flash-back_of_hydrogen_flames_on_perforated_plate_burners/links/5db950e9299bf1a47bfd948a/Quenching-and-flash-back-of-hydrogen-flames-on-perforated-plate-burners.pdf**, accessed 4 June 2024.
71 C. Movileanu, M. Mitu, V. Giurcan, D. Razus and D. Oancea, Quenching distances, minimum ignition energies and related properties of propane-air-diluent mixtures, *Fuel*, 2020, **274**, 117836.
72 A. C. Benim and B. Pfeiffelmann, Prediction of burning velocity and quenching distance of hydrogen flames, *E3S Web Conf.*, 2019, **128**, 1012.
73 Global Monitoring Laboratory, *Carbon Cycle Greenhouse Gases*, **https://gml.noaa.gov/ccgg/trends/**, accessed 22 December 2023.
74 S. Verhelst and T. Wallner, Hydrogen-fueled internal combustion engines, *Prog. Energy Combust. Sci.*, 2009, **35**, 490–527.
75 S. Eicheldinger, T. Bartkowski, A. Schröder, M. Prager and G. Wachtmeister, in *SAE Technical Paper Series*, SAE International, 400 Commonwealth Drive, Warrendale, PA, United States, 2019.
76 N. Peters and M. Bunce, Active Pre-Chamber as a Technology for Addressing Fuel Slip and its Associated Challenges to Lambda Estimation in Hydrogen ICEs, *JSAE/SAE Powertrains, Energy and Lubricants International*, 2023, DOI: **10.4271/2023-32-0041**.
77 S. G. Frankl, A. D. Gelner, S. Gleis, M. Härtl and G. Wachtmeister, in *ASME 2020 Power Conference*, American Society of Mechanical Engineers, 2020.